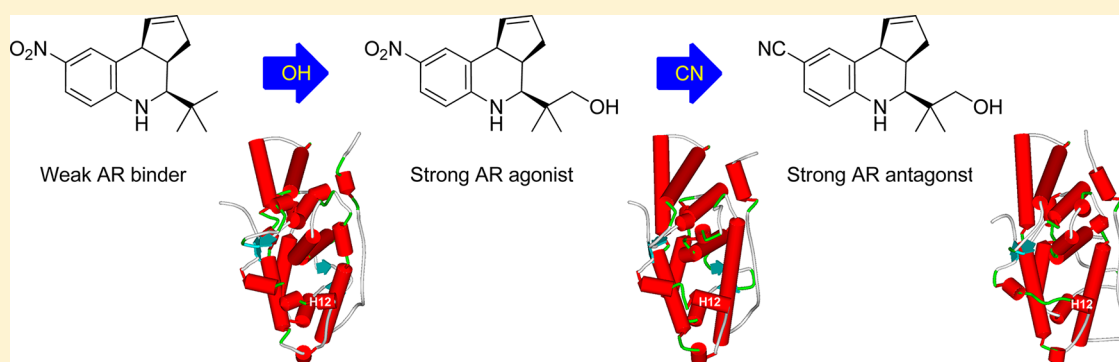


Subtle Structural Changes in Tetrahydroquinolines, A New Class of Nonsteroidal Selective Androgen Receptor Modulators, Induce Different Functions

Naoya Nagata,^{*,†} Kentaro Kawai,[†] and Isao Nakanishi^{*,‡}[†]Central Research Laboratories, Kaken Pharmaceutical Co., Ltd, 14, Shinomiya Minamikawara-cho, Yamashina, Kyoto 607-8042, Japan[‡]Department of Pharmaceutical Sciences, Kinki University, 3-4-1, Kowakae, Higashi-osaka, Osaka 577-8502, Japan

S Supporting Information



ABSTRACT: Tetrahydroquinolines (THQs), a new class of nonsteroidal selective androgen receptor (AR) modulators, have two indispensable functional groups, that is, a hydroxyl group for AR binding and a nitro group for agonistic activity. Interestingly, switching the nitro to a cyano group, the compound acts as an antagonist. To understand this phenomenon, molecular dynamics simulations were applied for dihydrotestosterone (DHT) and representative THQs complexes with AR. Upon ligand binding, the hydroxyl group formed a tight hydrogen-bond (H-bond) with Asn705 on Helix 3 (H3). The immobilization of Asn705 on H3 is helpful in the formation of tight H-bonds with Asp890 on loop 11–12, and this immobilization consequently leads to a stabilization of H12. The difference in the DHT carbonyl isosteres affected the presence or absence of the H-bonds between the hydroxyl group of THQ and Thr877 and the distortion of H12, which is caused by the methyl group of THQ. Thus, the binding, agonist, and antagonist functions were controlled by subtle structural changes in THQ.

INTRODUCTION

The androgen receptor (AR) is a member of the steroid hormone nuclear receptor (NR) superfamily, which consists of the estrogen, progesterone, glucocorticoid, and mineralocorticoid receptors.^{1–3} Binding of endogenous androgens, that is, testosterone (TES) and its active metabolite dihydrotestosterone (DHT), to AR plays an important role in the development and maintenance of the male reproductive system, muscle, bone, hair, larynx, skin, and lipid tissue.⁴ In females, the physiological roles for androgens are currently unknown; however, some reports suggest that androgens have an effect on libido, bone mineral density, and lean body mass.^{5,6} The biological effects of androgens are classified into two categories: the androgenic effect, which is the male reproductive system, and the anabolic effect, which is the growth of muscles and bones. The separation of these two effects and an increase in tissue selectivity may expand the therapeutic use of androgens.⁷ These AR modulators are referred to as selective androgen receptor modulators (SARMs), as is the case in the selective estrogen receptor modulators (SERMs).⁸ Various compounds,

such as GTx-007, LGD-2226, BMS-564929, and ACP-105, have been identified as SARMs from their preclinical studies, but the tissue-selectivity mechanism of SARMs is unclear (Chart 1).^{9–12}

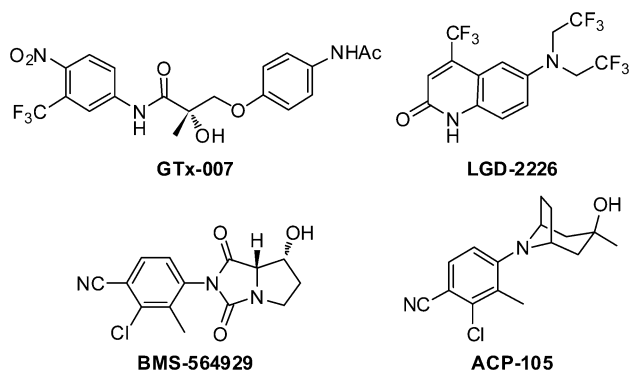
The mechanism of AR action is similar to that of other steroid hormone receptors.¹³ Ligand-unbound AR is mainly located in the cytoplasm and is associated with a complex of heat shock proteins (HSPs). Upon ligand binding, the AR dissociates from the HSPs and undergoes a conformational change, translocates to the nucleus, and dimerizes. In the nucleus, the AR binds to the androgen response element on the promoter or enhancer region of androgen responsive genes. The activated AR recruits various coregulators, which subsequently leads to the enhancement or transcription of the target genes.

A major conformational change of the AR occurs upon agonist binding: the rearrangement of helix 12 (H12) to occupy

Received: May 6, 2012

Published: July 13, 2012

Chart 1. Nonsteroidal AR Modulators



an appropriate position (the lid of the ligand-binding pocket). The aforementioned change is believed to trigger the coregulator recruitment from the NR structural data analyses.¹⁴ However, many of the NR antagonists possessed bulky side chains that cannot induce the H12 to the appropriate position directly (active antagonism).^{15,16} In cases where the antagonists lack bulky side chains, H12 stabilizes the inactive conformation indirectly (passive antagonism).¹⁷ In the case of the AR antagonist, hydroxyflutamide (HF) is considered to be a “passive antagonist” because it is comparable in size to TES and does not possess an obvious bulky side chain that acts as an active antagonist.¹⁸ Bisson et al. performed molecular dynamics (MD) simulations to demonstrate why HF switches its activity from antagonist to agonist upon T877A mutation.¹⁹ The HF was found to form two stable hydrogen bonds (H-bonds), that is, the amide side-chain of Asn705 on H3 and the guaninium side-chain Arg752 on H4, in both the AR wild type (WT) and the AR T877A mutant during 2.15 ns MD simulations. The HF that was bound into the AR WT agonist-like conformation introduced dynamic instability due to weaker interactions with the residues in H5, H11, and H12. In particular, the interaction between HF and Met895 on H12 was slightly different. The HF/AR WT complex displayed a weaker interaction pattern between HF and Met895 on H12 and a higher instability when compared to the AR T877A mutant. The HF/AR WT complex might stabilize a nonproductive receptor conformation upon HF binding.

In our previous reports, we showed that tetrahydroquinolines (THQs) are a new class of SARMs that were discovered on the basis of a ligand-based 3-D pharmacophore hypothesis (Table 1).^{20,21} Initially, compound 1 was designed to fulfill a three-point pharmacophore hypothesis (red, green, and magenta spheres), but it did not exhibit enough AR binding affinity. Subsequently, a four-point pharmacophore hypothesis (red, green, magenta, and cyan spheres) in which the corresponding hydroxyl group was added was used to redesign the structure. A nitro-containing THQ (NO₂-THQ 2, which was designed from the modified hypothesis, exhibits a strong AR binding affinity and agonistic activity (EC₅₀: 2.3 nM). Interestingly, the cyano-containing THQ (CN-THQ 4, the carbonyl isostere of which was changed from a nitro group to a cyano group, exhibited strong AR antagonistic activity (IC₅₀: 52 nM). NO₂-THQ 3, which exhibited improved water solubility, also had strong AR binding affinity and possessed agonistic activity (EC₅₀: 10 nM).²² Both compounds 2 and 3 had a high binding selectivity to the other steroid hormone receptors in the *in vitro* studies. Additionally, they had the desirable anabolic effects with weak undesirable effects on the accessory sex tissues in the *in vivo* rat osteoporosis model.^{21–23} Thus, these compounds had attractive profiles as SARM lead compounds.

From the structure activity relationship, the THQs have two indispensable functional groups, that is, a hydroxyl group for AR binding and a nitro group for agonistic activity. In an attempt to understand the role of these functional groups, MD simulations were performed using the GROMACS package,^{24,25} and the binding free energies (ΔG_{calc}) were calculated using the molecular mechanics/generalized Born surface area (MM/GBSA) method, which was included in the Schrödinger Suite.²⁶ At first, the plausible binding modes were estimated from the observed binding modes of THQs and the ΔG_{calc} values. Next, per-residue decomposed energetic analyses were performed to identify the important interactions and residues. These analyses are effective for the validation of the four-point pharmacophore hypothesis and the synthetic strategy of lead optimization. Finally, dynamic structural analyses were performed to understand the relationship between the subtle differences in the functional groups and their binding, agonist, and antagonist functions.

Table 1. AR Binding Affinities (IC₅₀), ΔG_{exp} Values, and ΔG_{calc} Values of DHT and THQs (kcal/mol)^a

ligand	IC ₅₀ ^b	ΔG_{exp} ^c	ΔG_{calc} ^d			
			Mode A	Mode B	Mode C	Mode D
DHT	3.1	−11.7	−54.9			
1	570	−8.6	−38.7	−36.5	−37.6	−33.1
2	13	−10.8	−45.9	−38.6	−42.1	−43.7
3	45	−10.1	−44.0	−38.5	−40.9	−39.4
4	140	−9.4	−43.5	−36.0	−30.8	−31.7

^aChemical structures of DHT and THQs (1–4), and putative pharmacophore points (spheres with the same color show the overlap). ^bBinding affinities (IC₅₀) were determined by rat AR competitive binding assay.^{21,22} ^c ΔG_{exp} values were calculated by the equation $\Delta G_{\text{exp}} = -RT \ln \text{IC}_{50}$.

^d ΔG_{calc} values are the means of the calculated results by Prime MM/GBSA module (1–2 ns).

MATERIALS AND METHODS

Ligand and Protein Preparation. The geometric optimization of the ligands was performed at a HF/6-31G* level using Gaussian 03.²⁷ RESP charges and AMBER ff99 force field were assigned to the ligand molecules using antechamber, which is a module of AMBER8.^{28–30} Protein structure of AR (1T7T) was obtained from the Protein Data Bank.³¹ All of the residues were protonated with the Protein Preparation Wizard, which is included in the Schrödinger Suite.²⁶

Ligand/AR Complexes Preparation. The initial structure of each complex is described below (Supporting Information Figure S1). The complex of DHT with AR was obtained from a cocrystallized structure; the 3-carbonyl group of DHT was located near Gln711 and Arg752 in AR, and the 17-hydroxyl group of DHT formed H-bonds with Asn705 and Thr877 in AR. Compounds 1–4 were arranged in four different initial complex structures (**Modes A–D**) by manual modeling to maximize the H-bonds within AR. **Mode A** was arranged so that the 6-nitro groups of THQ were located near the side chains of Gln711 and Arg752 in AR, the hydroxyl groups of 2–4 were located near the side chains of Asn705 and Thr877 in AR, and the 1-NH groups were located near the main-chain amide carbonyl of Leu704 in AR (Figure S1a). **Mode B** was arranged by flipping the THQ planes of **Mode A** so that the orientations around the 6-nitro and hydroxyl groups were kept, except for the 1-NH groups (Figure S1b). **Mode C** was arranged so that the hydroxyl groups of 2–4 were located near the side chains of Gln711 and Arg752 in AR, 6-nitro groups were located near the side chains of Asn705 and Thr877 in AR, and 1-NH groups were located near the main-chain amide of Leu704 in AR (Figure S1c). **Mode D** was arranged by flipping the THQ planes of **Mode C** so that the orientations around the 6-nitro and hydroxyl groups were kept except for the 1-NH groups, which was the same relation of the mode A with the mode B (Figure S1d).

MD Simulations. MD simulations were performed using the GROMACS 3.3 package with AMBER ff99 force field parameters and periodic boundary conditions.^{24,25} Protein–ligand complexes were solvated in 91 Å × 84 Å × 91 Å boxes with a density of 1 g/cm³, with the TIP3P water model.³² An appropriate number of counterions (Cl[−]) were added in the box to neutralize the systems. The temperature control was set using the Berendsen thermostat at 300 K, and pressure coupling was implemented using the Berendsen barostat with a constant pressure of 1 atm.³³ Nonbonded interactions were cutoff at 10 Å with updates at every five steps, and the particle mesh Ewald (PME) method was used for long-range electrostatic interactions.^{34,35} The LINCS procedure for covalent bond constraints was used.³⁶ MD simulations were performed with a constant-NPT ensemble. The energy of these complexes was minimized using the steepest descent approach and heating the system for 20 ps using the NVT ensemble. An equilibration step of 1 ns was followed by a production run of 1 ns, with a time step of 1.0 fs, and trajectories were collected every 0.5 ps. The total simulation time was 2 ns for each complex for binding mode selection. More 9 ns MD simulations were performed for dynamic structural analyses, and trajectories were collected every 10 ps.

Data Analysis. Each analysis was performed using the GROMACS module (g_rms, g_hbond, g_dist, g_angle) and MD trajectories (1–2 ns, and 0–11 ns).^{24,25} Binding free energies (ΔG_{calc}), interaction energies per residue, Coulomb

term (ΔE_{Coul}), and vdW term (ΔE_{vdW}) were calculated using the MM/GBSA method, which was included in the Schrödinger Suite²⁶ and MD trajectories.

RESULTS AND DISCUSSION

MD Simulations. The initial complex structure of DHT/AR was used for the cocrystallized structure (1T7T).³¹ Four different initial complex structures of THQ/AR were prepared (preparation described in the previous section). Two initial THQs structures (**Modes A** and **B**) were arranged to satisfy the four-point pharmacophore hypothesis (Supporting Information Figure S1a,b). These functional groups could potentially establish H-bonds with each of the corresponding residues. The other two initial structures (**Modes C** and **D**) were arranged upside down as compared to **Modes A** and **B** (Figure S1c,d). Before starting the trajectory analyses, we confirmed that the simulation was normally terminated by the root-mean-square deviation (rmsd) analyses (Supporting Information Figures S2–S4). The rmsd values of the protein backbone and the ligand-heavy atoms were investigated in the simulation. The complex structures were thought to reach equilibrium after 300 ps. The rmsd values of all of the complexes (DHT and THQs 1–4, **Modes A–D**) during the simulations of 2 ns were 1.0–1.5 Å for the protein backbone and 0.2–0.6 Å for the ligand-heavy atoms. To obtain a plausible binding mode, the mean ΔG_{calc} values were calculated on the basis of the 2000 snapshots at 1–2 ns (Table 1). To perform further dynamic structural analyses, longer MD simulations were conducted for the five **Mode A** complexes of DHT and THQ 1–4 with AR (total 11 ns). The rmsd values were 1.1–1.4 Å for the protein backbone and 0.1–0.7 Å for the ligand-heavy atoms, and the mean ΔG_{calc} values were calculated from the 2000 snapshots at 0–11 ns.

The Plausible Binding Mode. For each THQ, the most plausible binding mode was selected from the aforementioned four complexes, which was based on the observed binding modes of THQ and the ΔG_{calc} values (Table 1).

At first, the observed binding modes were determined as follows. In the case of **Mode A**, the 6-nitro and/or cyano groups are stabilized by the Coulomb interactions with the hydrophilic residues, Gln711 and Arg752, the 1-NH groups form a tight H-bond with the main-chain amide carbonyl of Leu704, and the aromatic parts of THQ rings interact with the aromatic side-chain of Phe764 through edge-to-face aromatic interaction. The hydroxyl groups of 2–4 form a tight H-bond with the side-chain amide carbonyl of Asn705. The van der Waals (vdW) interactions with the hydrophobic residues inside the ligand-binding pocket contribute to the ligand stabilization.

In the case of **Mode B**, the 6-nitro and/or cyano groups are also stabilized by the Coulomb interactions with the hydrophilic residues, Gln711 and Arg752, but the 1-NH groups could not form any H-bonds with the main-chain amide carbonyl of Leu704 throughout the MD simulations by flipping the THQ plane against the **Mode A**. The presence or absence of hydrogen bonding (H-bonding) with Leu704 directly affected the strength of the $\Delta \Delta G_{\text{calc}}$ values (2, 7.3 kcal/mol; 3, 5.5 kcal/mol; 4, 7.5 kcal/mol, respectively), although the Coulomb and vdW interactions were similar to those of **Mode A**.

In the case of **Mode C**, a probable binding mode was not obtained. Compound 2 was stabilized thorough three H-bonds with Leu704, Gln711, and Thr877, and compound 3 was stabilized thorough two H-bonds with Leu704 and Thr877. The binding modes of 4 were unstable because only two or less H-bonds were observed during the MD simulations.

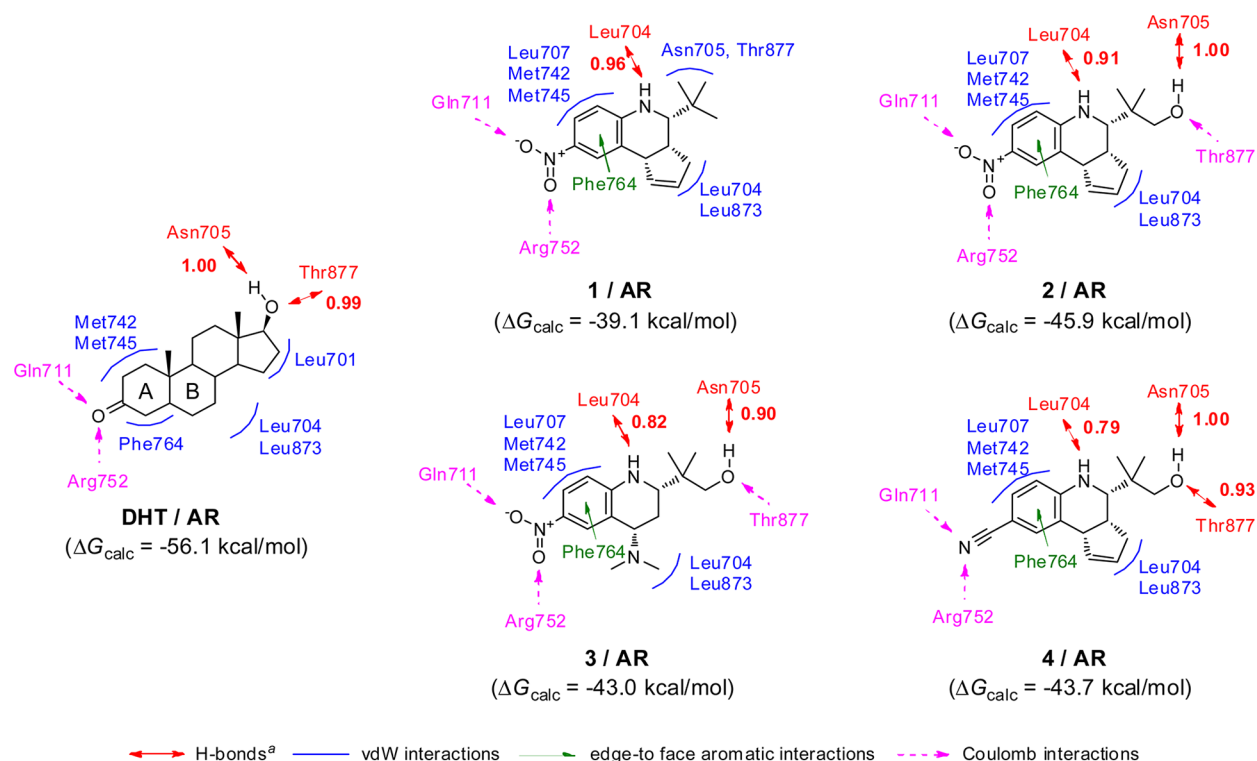


Figure 1. Most plausible binding mode of the SARM and interaction residues (**Mode A**). ^aThe number near the H-bond arrows show the hydrogen bonding frequency during the MD simulations.

In the case of **Mode D**, a probable binding mode was also not obtained. H-bonding between hydroxyl group and the amide side-chain of Gln711 was observed with compound **2** but was not observed with the others. The nitro and cyano groups did not form H-bonds with AR. The ligand was not sufficiently stabilized by H-bonding within their ligand binding pocket.

The ΔG_{calc} values of **Mode A** were the lowest among the four binding modes. The order of the activity strengths of **Mode A** reproduced the ΔG_{exp} values ($\text{DHT} < 2 < 3 < 4 < 1$), but **Modes B, C, and D** did not exhibit the same ΔG_{calc} values in their ΔG_{exp} values ($\text{DHT} < 2 < 3 < 1 < 4$).

Consequently, **Mode A** was the most plausible binding mode among the four binding modes, the ΔG_{calc} values, and the correlation coefficient between the values of ΔG_{calc} and ΔG_{exp} ($R^2 = 0.88$) was the highest among the four binding modes. Additionally, **Mode A** satisfied our four-point pharmacophore hypothesis. In the following sections, we used the results of the 11 ns MD simulations to analyze the dynamic structural changes in detail. The mean ΔG_{calc} values of the 11 ns MD simulations were almost the same as those of the shorter MD simulations (DHT, -56.1 kcal/mol; **1**, -39.1 kcal/mol; **2**, -45.9 kcal/mol; **3**, -43.0 kcal/mol; **4**, -43.7 kcal/mol, respectively).

Interaction Energy Analysis. Per-residue decomposition analyses were performed to evaluate the energetic influences and the H-bonds of critical residues on the binding of DHT and THQs with AR (Figure 1, Supporting Information Table S1 and Figure S5).

The functional groups at both ends of DHT, that is, the 3-carbonyl group and the 17-hydroxyl group, were stabilized by strong Coulomb interactions with the four hydrophilic residues, Asn705, Gln711, Arg752, and Thr877. The 3-carbonyl oxygen was stabilized through the Coulomb interaction with the amide side-chain of Gln711 and the guanidinium side-chain of

Arg752. The 17-hydroxyl groups formed two tight H-bonds with the amide side-chain of Asn705 and the hydroxyl side-chain of Thr877 (the H-bond frequencies were 1.00 and 0.99, respectively). These four interactions contributed to the stabilization inside the ligand-binding pocket. The A and B rings of DHT were surrounded by five hydrophobic residues, that is, Leu704, Met742, Met745, Phe764, and Leu873, and this result was confirmed by crystallographic analysis.^{31,37} Additionally, the key H-bonds of DHT turned out to be those between the 17-hydroxyl group and Asn705 on H3 and/or Thr877 on H11.

The NO₂-THQs **1–3** were stabilized by their interactions with three hydrophilic residues, that is, Asn705, Gln711, and Arg752, and with five hydrophobic residues, that is, Leu704, Leu707, Met742, Met745, and Phe764. The 6-nitro group was stabilized through the Coulomb interaction with the side-chains of Gln711 and Arg752. The 1-NH group formed a tight H-bond with the main-chain amide carbonyl of Leu704 (0.82–0.96). The THQ rings constituted an edge-to-face aromatic interaction with the aromatic side-chain of Phe764.

The cyclopentene moiety of **1** and **2** was stabilized within a hydrophobic subpocket that was unoccupied by DHT. The H-bond frequency between **1** and AR was 1.10. The hydroxyl group of **2** formed a tight H-bond with the amide side-chain of Asn705 (0.91), and the H-bond frequency between **2** and AR was 2.86. Interestingly, this hydroxyl group was designed by mimicking the 17-hydroxyl group of DHT, but it only formed one H-bond with Asn705.

The hydroxyl group of **3** also formed tight H-bonds with Asn705 (0.90). Similar to **1** and **2**, the *N,N*-dimethylamino group was stabilized by vdW interactions with the hydrophobic side-chain of both Leu704 and Leu873. Their interactions are similar to those of the other THQs. The H-bond frequency between **3** and AR was 2.55.

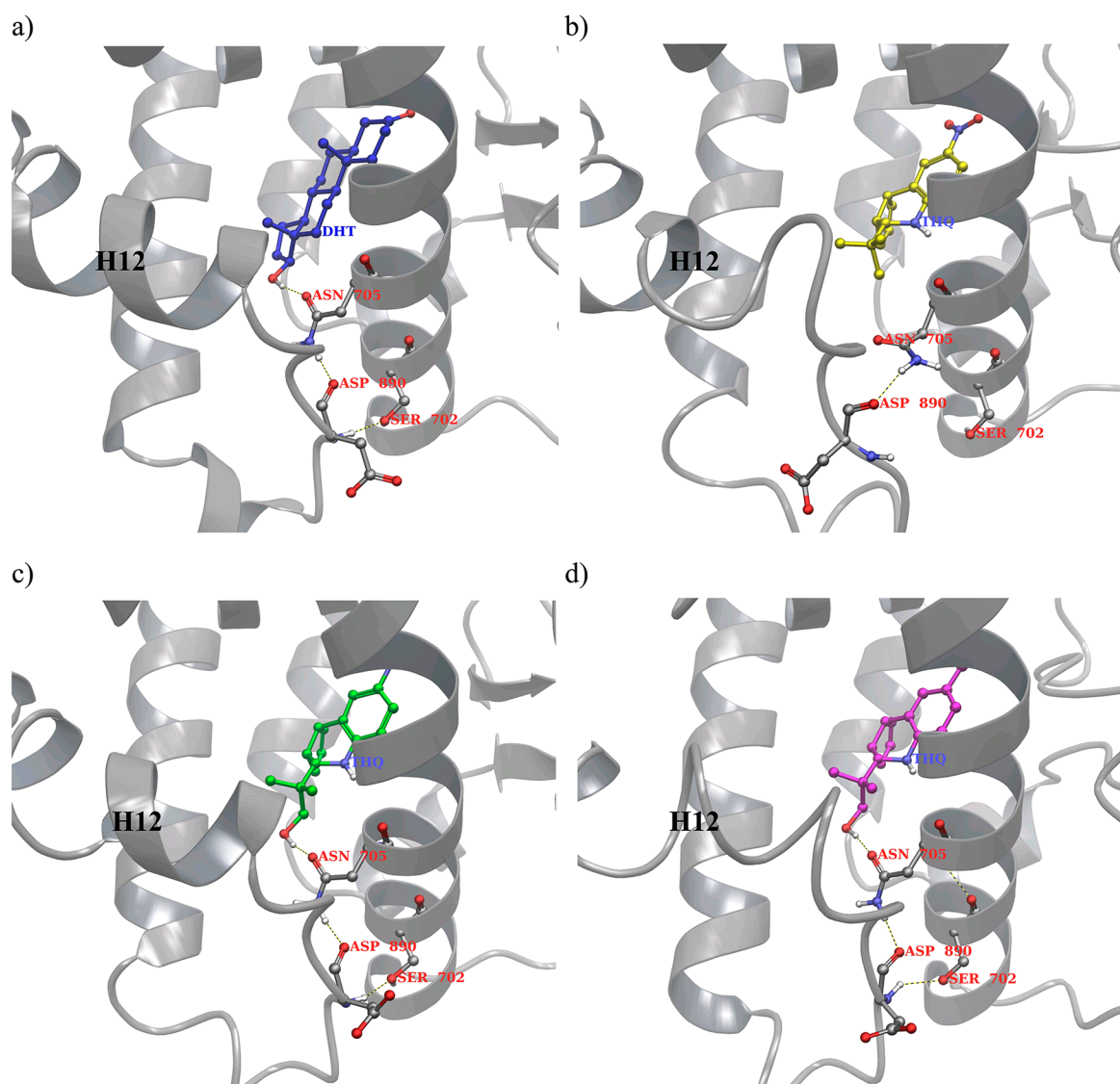


Figure 2. The H-bonding network involving ligand–Asn705, Asp890–Asn705, and Asp890–Ser702 (dashed lines represent H-bonds). Snapshots of the THQ–AR complexes at the end of 11 ns MD simulations: (a) cocrystallized DHT/AR complex (blue), (b) 1/AR complex (yellow), (c) 2/AR complex (green), and (d) 4/AR complex (magenta).

Compound **4** was also stabilized by the interaction with three hydrophilic residues, that is, Asn705, Gln711, and Arg752, and five hydrophobic residues, that is, Leu704, Leu707, Met742, Met745, and Phe764, which was similar to the stability observed with NO₂-THQ. The 6-cyano group of **4** was stabilized through the Coulomb interaction with the side chains of Gln711 and Arg752. The 1-NH group of the THQ ring forms a tight H-bond with the main-chain amide carbonyl of Leu704 (0.79). The THQ ring has an edge-to-face aromatic interaction with Phe764, and the cyclopentene moiety was stabilized within the hydrophobic subpocket. The hydroxyl group of CN-THQ **4** created two tight H-bonds with the amide side-chain of Asn705 (1.00) and the hydroxyl side-chain of Thr877 (0.93). The H-bond frequency between **4** and AR was 3.19. We found that the hydroxyl group of CN-THQ **4** behaved differently from NO₂-THQ (**2** and **3**), despite their similar design.

Interestingly, the presence or absence of the hydroxyl group affected the AR binding affinity directly. The behavior of the hydroxyl group was quite different between the THQs.

Specifically, the NO₂-THQs established only one H-bond with Asn705, and the CN-THQ established two H-bonds with Asn705 and Thr877.

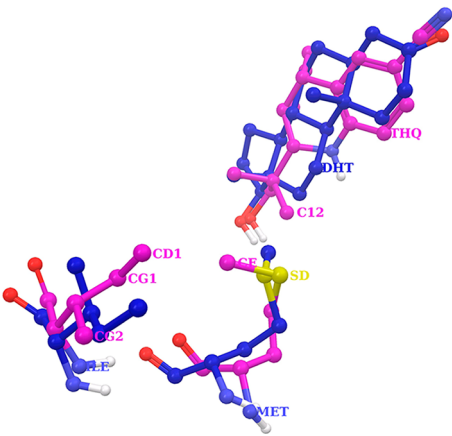
Subtle Structural Changes of THQ Induced Different Functions. From the analysis of the R1881/AR cocrystallized structure, Matias et al. showed that the H-bond between Asn705 and the hydroxyl group of the ligand stimulate H-bond formation between Asn705 and Asp890, which leads to the stabilization of loop 11–12 (L11–12).³⁷ Asn705 on H3 also forms two H-bonds with the hydrogen atom of the 17-hydroxyl group in DHT and the main-chain amide carbonyl of Asp890 on L11–12 with the initial DHT/AR complex (Figure 2a). Additionally, the hydroxyl group of the side chain of Ser702 on H3 forms one H-bond with main-chain amide hydrogen of Asp890. Thus, one H-bond between the hydroxyl group of the ligand and Asn705 and two H-bonds between L11–12 (Asp890) and H3 (Asn705 and Ser702) contributed to the stabilization of the conformation of H12. To elucidate the relationship between the H-bonding network and ligand binding, we analyzed the dynamic structural changes in detail

(Figure 2b–d). In the case of compound **1**, which lacks a hydroxyl group, only the H-bond between Asp890 and Asn705 was kept (H-bond frequency; 0.85), and the other two possible H-bonds were not observed during the MD simulations. Thus, this H-bonding network might be disrupted throughout the simulation (0.88). However, in the case of compounds **2–4**, which possessed hydroxyl groups, this H-bonding network was maintained throughout the simulations (**2**, 2.38; **3**, 2.42; **4**, 2.71, respectively). The H-bonding between THQ and Asn705 is necessary for ligand binding, and the H-bonding between L11–12 (Asp890) and H3 (Asn705 and Ser702) might be necessary for the stabilization of L11–12 and H12 folding. Consequently, the hydroxyl group of the ligands played an important role in maintaining the H-bonding network; therefore, the hydroxyl groups of THQs are indispensable for binding to AR.

The NO₂-THQs **2** and **3** act as agonists, but the CN-THQ **4** acts as antagonist toward the AR. These functional groups are well-known DHT carbonyl isosteres. We examined the different behaviors of THQs. Gln711 and Arg752 are the potential residues that are responsible for creating H-bonds with the nitro/cyano groups. Although the nitro group is a bidentate functional group, only one H-bond through the Gln711 was slightly observed during the simulation. Thus, this difference does not have an effect on the agonist and/or antagonist function. However, the H-bond between the hydroxyl group of THQs and AR showed a different behavior. The hydroxyl group of NO₂-THQs **2** and **3** formed only one H-bond with the side chain of Asn705 (**2**, 1.00; **3**, 0.90). However, the hydroxyl group of CN-THQ **4** formed two H-bonds with the side chains of Asn705 and Thr877 (**4**, 1.93). The length from the nitro/cyano group to hydroxyl group in the THQs might cause this difference. Specifically, the CN-THQ (**4**; 11.39 Å) was slightly longer than the NO₂-THQs (**2** and **3**; both 10.51 Å). This H-bond regulates the location of the two methyl groups of THQ. Bisson et al. showed that Met895 (located in H12) destabilization by the sulfonyl linkage of (*R*)-Bicartamide might be related to the antagonist function, as determined by measuring the interatomic distances between the sulfonyl oxygen and side chain of Met895.¹⁹ To elucidate the effect of H12 destabilization by the methyl group of CN-THQ **4**, we compared the average interatomic distances between the C12 methyl group of THQ and the side chain of Met895 (Table 2). The average distances between the C12 methyl group of antagonist **4** and Met895 S_δ, C_ε atoms are 4.85, 7.34 Å. However, the corresponding distances of agonist **2** and **3** and Met895 were 4.31, 6.69 Å, and 4.36, 7.06 Å, respectively. The C12 methyl group of antagonist **4** stimulated a movement of the Met895 C_ε atom to the opposite side of the initial structure. During the simulations of the **4**/AR complex, the Met895 C_ε atom was found to stabilize the hydrophobic side-chain of Ile898 (Table 2, Supporting Information Figure S6).

This hydrophobic interaction led to the collapse of the H12 helix. The φ - ψ angle of the Ile898 and Ile899 within H12, the rmsd of H12, and the H-bond frequency within H12 supported the above results (Supporting Information Table S2, Figures S7 and S8). The average φ - ψ angle of most of the residues on H12 was within the ideal range or near the initial cocrystallized structures. However, the average φ - ψ angle of Ile898 (−99.2, 6.1) and the φ angle of Ile899 (−113.0) were outside of the ideal angle range. The rmsd values of H12 were bound to NO₂-THQ **2** and **3** were 0.51 and 0.53 Å, respectively, and the rmsd of H12 that was bound to CN-THQ **4** was 0.76 Å. The H12

Table 2. Average Distances (Å) between THQs and Met895 and between Met895 and Ile898^a



ligand	THQ C12–Met895 ^b		Met895 C _ε –Ile898 ^c		
	S _δ	C _ε	C _γ	C _{δ1}	C _{δ2}
DHT ^d			7.70	8.08	7.53
2	4.31	6.69	6.61	6.82	5.91
3	4.36	7.06	6.08	6.29	4.72
4	4.85	7.34	4.71	5.15	7.16

^aComparison of the initial structure of the DHT/AR complex (blue) with the last snapshot of the CN-THQ **4**/AR complex (magenta).

^bThe first and second columns show the average distance between the C12 methyl group of THQ and S_δ, C_ε of Met895, respectively. ^cThe third, fourth, and fifth columns show the average distance between C_ε of Met895 and C_γ, C_{δ1}, and C_{δ2} of Ile898, respectively. ^dThe row of DHT represents the corresponding distances in the initial cocrystallized structure.

helix (Pro892–Ser908) of the cocrystallized structure constructed 12 H-bonds within the helix. The H-bonding frequencies within the H12 bound to NO₂-THQ **2** and **3** were 11.12 and 11.13, respectively. However, the H-bonding frequency within the H12 that was bound with CN-THQ **4** was 9.89. The H-bond frequency within H12 was clearly reduced when CN-THQ was bound to the AR agonist form. These results suggested that CN-THQ bound to the AR agonist form caused a H12 distortion during the MD simulations. We examined the last snapshot of the complex CN-THQ **4** with AR by several structural viewers, and we observed that part of the region (Ala896–Pro905) of H12 was no longer a helix structure (Figure 3). In the CN-THQ/AR complex, part of the hydrogen bonds within H12 were lost, and new hydrogen bonds formed with water molecules stabilized the distorted structure instead. Thus, the presence or absence of H-bonding between the hydroxyl group of THQ and Thr877 regulated the location of the methyl group of THQ and induced H12 distortion during the MD simulation. From the aforementioned, we deduced that H12 folding might prefer an antagonist form upon CN-THQ binding to AR. We assumed that this observation was the reason that CN-THQ exhibits an antagonist function. Additionally, the difference in the carbonyl isosteres was caused by the agonist and/or antagonist functions of THQs indirectly.

CONCLUSION

In the present study, MD simulations of DHT or THQs complexes with AR were performed to assess their binding modes and protein structural changes. The plausible binding

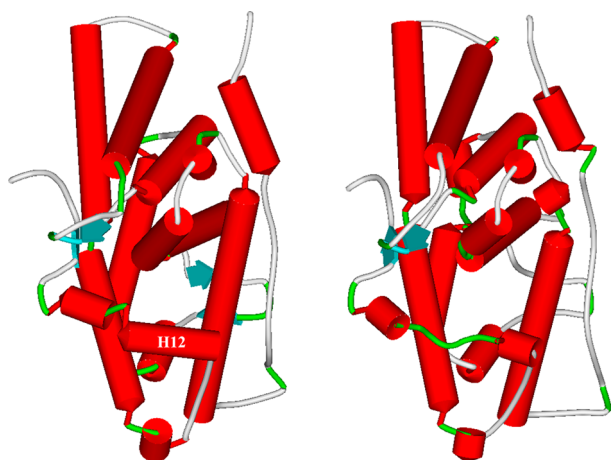


Figure 3. Graphical representation of the cocrystallized structure (left) and last snapshot of the CN-THQ/AR complex (right): α -helices are shown as red cylinders, and β -sheets are shown as cyan arrows.

modes were determined from the observed binding mode of THQs and the ΔG_{calc} values as calculated by the MM/GBSA method. This estimated binding mode was coincident with our initial four-point pharmacophore hypothesis. Compound **2**, which was the most active among all of the THQs, showed the best fit within the ligand binding pocket of AR, and it took into account the three H-bonding network, Coulomb interactions, and vdW interactions. The cyclopentene moiety was stabilized within the hydrophobic subpocket that is unused by steroidal analogues and is more stable than the *N,N*-dimethylamino group of **3**.

The H-bonds among the hydroxyl groups of THQs, Asn705, Asp890, and Ser702 are important for binding. This H-bonding network may stabilize the location of H3 and L11–12, and this network may be necessary for H12 relocation upon strong AR ligand binding. The C12 methyl group of CN-THQ might preclude H12 relocation. The results of these analyses suggest that the subtle differences of the functional group should affect the binding, agonist, and antagonist function of THQs.

■ ASSOCIATED CONTENT

● Supporting Information

A pdf file contains Figures S1–S8 and Tables S1 and S2. Figure S1 shows the initial ligand binding mode of MD simulations, Figures S2–S4 show the rmsd of the protein backbone and the ligand-heavy atoms of the complexes ligand (DHT and THQs) with AR during the MD simulations (0–2 ns and 0–11 ns), Table S1 shows the interaction energy, ΔE_{Coulb} and ΔE_{vdW} values between the ligands (DHT and THQs) and the critical residues of AR, Figure S5 shows the lowest energy complexes DHT and THQs with AR, Figure S6 shows the cumulative average of interatomic distances between the C12 methyl group of THQ and the C_{γ} atom of Ile898 during the MD simulations (0–11 ns), Table S2 shows the average ϕ – ψ angles of representative residue of H12, Figure S7 shows the cumulative average of the rmsd of the H12 backbone (Pro892–Ser908) during the MD simulations (0–11 ns), and Figure S8 shows the cumulative average of the hydrogen-bond frequency of the H12 during the MD simulations (0–11 ns). This material is available free of charge via the Internet at <http://pubs.acs.org>.

■ AUTHOR INFORMATION

Corresponding Author

*Tel.: +81-75-594-0787 (N.N.); +81-6-6721-2332 (I.N.). E-mail: nagata_naoya@kaken.co.jp (N.N.); isayan@phar.kindai.ac.jp (I.N.).

Notes

The authors declare no competing financial interest.

■ ACKNOWLEDGMENTS

We thank Dr. Kiyoshi Inoguchi and Dr. Hajime Kamachi for their support.

■ ABBREVIATIONS

SARM, selective androgen receptor modulator; THQ, tetrahydroquinoline; AR, androgen receptor; DHT, dihydrotestosterone; H-bond, hydrogen bond; NR, nuclear receptor; MD, molecular dynamics; MM/GBSA, molecular mechanics/generalized Born surface area; PME, particle mesh Ewald; LINCS, linear constraint solver; rmsd, root-mean-square deviation

■ REFERENCES

- (1) Mohler, M. L.; Bohl, C. E.; Jones, A.; Coss, C. C.; Narayanan, R.; He, Y.; Hwang, D. J.; Dalton, J. T.; Miller, D. D. Nonsteroidal selective androgen receptor modulators (SARMs): dissociating the anabolic and androgenic activities of the androgen receptor for therapeutic benefit. *J. Med. Chem.* **2009**, *52*, 3597–3617.
- (2) Narayanan, R.; Mohler, M. L.; Bohl, C. E.; Miller, D. D.; Dalton, J. T. Selective androgen receptor modulators in preclinical and clinical development. *Nucl. Recept. Signaling* **2008**, *6*, e010.
- (3) Gao, W.; Bohl, C. E.; Dalton, J. T. Chemistry and structural biology of androgen receptor. *Chem. Rev.* **2005**, *105*, 3552–3370.
- (4) Takeda, H.; Chodak, G.; Mutchnik, S.; Nakamoto, T.; Chang, C. Immunohistochemical localization of androgen receptors with mono- and polyclonal antibodies to androgen receptor. *J. Endocrinol.* **1990**, *126*, 17–25.
- (5) Davis, S. Androgen replacement in women: a commentary. *J. Clin. Endocrinol. Metab.* **1999**, *84*, 1886–1891.
- (6) Davis, S. R. The therapeutic use of androgens in women. *J. Steroid Biochem. Mol. Biol.* **1999**, *69*, 177–184.
- (7) Rosen, J.; Negro-Vilar, A. Novel, non-steroidal, selective androgen receptor modulators (SARMs) with anabolic activity in bone and muscle and improved safety profile. *J. Musculoskeletal Neuronal Interact.* **2002**, *2*, 222–224.
- (8) Tobias, S. C.; Qiu, J.; Kelly, M. J.; Scanlan, T. S. Synthesis and biological evaluation of SERMs with potent nongenomic estrogenic activity. *ChemMedChem* **2006**, *1*, 565–571.
- (9) Kim, J.; Wu, D.; Hwang, D. J.; Miller, D. D.; Dalton, J. T. The para substituent of S-3-(phenoxy)-2-hydroxy-2-methyl-N-(4-nitro-3-trifluoromethyl-phenyl)-propionamides is a major structural determinant of in vivo disposition and activity of selective androgen receptor modulators. *J. Pharmacol. Exp. Ther.* **2005**, *315*, 230–239.
- (10) Miner, J. N.; Chang, W.; Chapman, M. S.; Finn, P. D.; Hong, M. H.; López, F. J.; Marschke, K. B.; Rosen, J.; Schrader, W.; Turner, R.; van Oeveren, A.; Viveros, H.; Zhi, L.; Negro-Vilar, A. An orally active selective androgen receptor modulator is efficacious on bone, muscle, and sex function with reduced impact on prostate. *Endocrinology* **2007**, *148*, 363–373.
- (11) Ostrowski, J.; Kuhns, J. E.; Lupisella, J. A.; Manfredi, M. C.; Beehler, B. C.; Krystek, S. R., Jr.; Bi, Y.; Sun, C.; Seethala, R.; Golla, R.; Sleph, P. G.; Fura, A.; An, Y.; Kish, K. F.; Sack, J. S.; Mookhtiar, K. A.; Grover, G. J.; Hamann, L. G. Pharmacological and X-ray structural characterization of a novel selective androgen receptor modulator: potent hyperanabolic stimulation of skeletal muscle with hypostimulation of prostate in rats. *Endocrinology* **2007**, *148*, 4–12.
- (12) Miller, C. P.; Shomali, M.; Lyttle, C. R.; O'Dea, L. S.; Herendeen, H.; Gallacher, K.; Paquin, D.; Compton, D. R.; Sahoo, B.;

- Kerrigan, S. A.; Burge, M. S.; Nickels, M.; Green, J. L.; Katzenellenbogen, J. A.; Tchesnokov, A.; Hattersley, G. Design, synthesis, and preclinical characterization of the selective androgen receptor modulator (SARM) RAD140. *ACS Med. Chem. Lett.* **2011**, *2*, 124–129.
- (13) Gronemeyer, H.; Gustafsson, J. Å.; Laudet, V. Principles for modulation of the nuclear receptor superfamily. *Nat. Rev. Drug Discovery* **2004**, *3*, 950–964.
- (14) Renaud, J. P.; Moras, D. Structural studies on nuclear receptors. *Cell. Mol. Life Sci.* **2000**, *57*, 1748–1769.
- (15) Steinmetz, A. C.; Renaud, J. P.; Moras, D. Binding of ligands and activation of transcription by nuclear receptors. *Annu. Rev. Biophys. Biomol. Struct.* **2001**, *30*, 329–359.
- (16) Weatherman, R. V.; Fletterick, R. J.; Scanlan, T. S. Nuclear-receptor ligands and ligand-binding domains. *Annu. Rev. Biochem.* **1999**, *68*, 559–581.
- (17) Shiau, A. K.; Barstad, D.; Radek, J. T.; Meyers, M. J.; Nettles, K. W.; Katzenellenbogen, B. S.; Katzenellenbogen, J. A.; Agard, D. A.; Greene, G. L. Structural characterization of a subtype-selective ligand reveals a novel mode of estrogen receptor antagonism. *Nat. Struct. Biol.* **2002**, *9*, 359–364.
- (18) Singh, S. M.; Gauthier, S.; Labrie, F. Androgen receptor antagonists (antiandrogens): structure-activity relationships. *Curr. Med. Chem.* **2000**, *7*, 211–247.
- (19) Bisson, W. H.; Abagyan, R.; Cavasotto, C. N. Molecular basis of agonicity and antagonicity in the androgen receptor studied by molecular dynamics simulations. *J. Mol. Graphics Modell.* **2008**, *4*, 452–458.
- (20) Harris, D.; Clayton, T.; Cook, J.; Sahbaie, P.; Halliwell, R. F.; Furtmüller, R.; Huck, S.; Sieghart, W.; DeLorey, T. M. Selective influence on contextual memory: physiochemical properties associated with selectivity of benzodiazepine ligands at GABA_A receptors containing the $\alpha 5$ subunit. *J. Med. Chem.* **2008**, *51*, 3788–3803.
- (21) Nagata, N.; Miyakawa, M.; Amano, S.; Furuya, K.; Yamamoto, N.; Inoguchi, K. Design and synthesis of tricyclic tetrahydroquinolines as a new series of nonsteroidal selective androgen receptor modulators (SARMs). *Bioorg. Med. Chem. Lett.* **2011**, *21*, 1744–1747.
- (22) Nagata, N.; Miyakawa, M.; Amano, S.; Furuya, K.; Yamamoto, N.; Nejishima, H.; Inoguchi, K. Tetrahydroquinolines as a novel series of nonsteroidal selective androgen receptor modulators: Structural requirement for better physicochemical and biological properties. *Bioorg. Med. Chem. Lett.* **2011**, *21*, 6310–6313.
- (23) Hanada, K.; Furuya, K.; Yamamoto, N.; Nejishima, H.; Ichikawa, K.; Nakamura, T.; Miyakawa, M.; Amano, S.; Sumita, Y.; Oguro, N. Bone anabolic effects of S-40503, a novel nonsteroidal selective androgen receptor modulator (SARM), in rat models of osteoporosis. *Biol. Pharm. Bull.* **2003**, *26*, 1563–1569.
- (24) Berendsen, H. J. C.; van der Spoel, D.; van Drunen, R. GROMACS: a message-passing parallel molecular dynamics implementation. *Comput. Phys. Commun.* **1995**, *91*, 43–57.
- (25) Lindahl, E.; Hess, B.; van der Spoel, D. GROMACS 3.0: A package for molecular simulation and trajectory analysis. *J. Mol. Model.* **2001**, *7*, 306–317.
- (26) Schrödinger Suite 2010; Maestro, version 9.0; Prime MM-GBSA, version 1.4.1; Schrödinger, LLC: New York, NY, 2010.
- (27) Frisch, M. J.; Trucks, G. W.; Schlegel, H. B.; Scuseria, G. E.; Robb, M. A.; Cheeseman, J. R.; Montgomery, J. A., Jr.; Vreven, T.; Kudin, K. N.; Burant, J. C.; Millam, J. M.; Iyengar, S. S.; Tomasi, J.; Barone, V.; Mennucci, B.; Cossi, M.; Scalmani, G.; Rega, N.; Petersson, G. A.; Nakatsuji, H.; Hada, M.; Ehara, M.; Toyota, K.; Fukuda, R.; Hasegawa, J.; Ishida, M.; Nakajima, T.; Honda, Y.; Kitao, O.; Nakai, H.; Klene, M.; Li, X.; Knox, J. E.; Hratchian, H. P.; Cross, J. B.; Adamo, C.; Jaramillo, J.; Gomperts, R.; Stratmann, R. E.; Yazyev, O.; Austin, A. J.; Cammi, R.; Pomelli, C.; Ochterski, J. W.; Ayala, P.; Morokuma, K.; Voth, G. A.; Salvador, P.; Dannenberg, J. J.; Zakrzewski, V. G.; Dapprich, S.; Daniels, A. D.; Strain, M. C.; Farkas, O.; Malick, D. K.; Rabuck, A. D.; Raghavachari, K.; Foresman, J. B.; Ortiz, J. V.; Cui, J. Q.; Baboul, A. G.; Clifford, S.; Cioslowski, J.; Stefanov, B. B.; Liu, G.; Liashenko, A.; Piskorz, P.; Komaromi, I.; Martin, R. L.; Fox, D. J.; Keith, T.; Al-Laham, M. A.; Peng, C. Y.; Nanayakkara, A.; Challacombe, M.; Gill, P. M. W.; Johnson, B.; Chen, W.; Wong, M. W.; Gonzalez, C.; Pople, J. A. *Gaussian 03*, revision C.02; Gaussian, Inc.: Wallingford, CT, 2004.
- (28) Wang, J.; Cieplak, P.; Kollman, P. A. How well does a restrained electrostatic potential (RESP) model perform in calculating conformational energies of organic and biological molecules? *J. Comput. Chem.* **2000**, *21*, 1049–1074.
- (29) Bayly, C. I.; Cieplak, P.; Cornell, W.; Kollman, P. A. A well-behaved electrostatic potential based method using charge restraints for deriving atomic charges: The RESP model. *J. Phys. Chem.* **1993**, *97*, 10269–10280.
- (30) Wang, J.; Wolf, R. M.; Caldwell, J. W.; Kollman, P. A.; Case, D. A. Development and testing of a general amber force field. *J. Comput. Chem.* **2004**, *25*, 1157–1174.
- (31) Hur, E.; Pfaff, S. J.; Payne, E. S.; Grøn, H.; Buehrer, B. M.; Fletterick, R. J. Recognition and accommodation at the androgen receptor coactivator binding interface. *PLoS Biol.* **2004**, *2*, 1303–1312.
- (32) Jorgensen, W. L.; Chandrasekhar, J.; Madura, J. D.; Impey, R. W.; Klein, M. L. Comparison of simple potential functions for simulating liquid water. *J. Chem. Phys.* **1983**, *79*, 926–935.
- (33) Berendsen, H. J. C.; Postma, J. P. M.; van Gunsteren, W. F.; DiNola, A.; Haak, J. R. Molecular dynamics with coupling to an external bath. *J. Chem. Phys.* **1984**, *81*, 3684–3690.
- (34) Darden, T.; York, D.; Pedersen, L. Particle mesh Ewald: An $N \log(N)$ method for Ewald sums in large system. *J. Chem. Phys.* **1993**, *98*, 10089–10092.
- (35) Essman, U.; Perera, L.; Berkowitz, M. L.; Darden, T.; Lee, H.; Pedersen, L. G. A smooth particle mesh Ewald method. *J. Chem. Phys.* **1995**, *103*, 8577–8593.
- (36) Hess, B.; Bekker, H.; Berendsen, H. J. C.; Fraaije, J. G. E. M. LINCS: A linear constraint solver molecular simulations. *J. Comput. Chem.* **1997**, *18*, 1463–1472.
- (37) Matias, P. M.; Donner, P.; Coelho, R.; Thomaz, M.; Peixoto, C.; Macedo, S.; Otto, N.; Joschko, S.; Scholz, P.; Wegg, A.; Bäsler, S.; Schäfer, M.; Egner, U.; Carrondo, M. A. Structural evidence for ligand specificity in the binding domain of the human androgen receptor. Implications for pathogenic gene mutations. *J. Biol. Chem.* **2000**, *275*, 26164–26171.